agronomy

MDPI

Article

Enhanced Soil Moisture Management Using Waste Green Algae-Derived Polymers: Optimization of Application Rate and Mixing Depth

Zijian He [1,2,3,†], Jiaping Liang [1,2,3,4,5,*,†], Yanwei Lu [1,2,3], Qiliang Yang [4,5], Chengmei Lu [4,5] and Die Wu [4,5]

[1] School of Water and Environment, Chang'an University, Xi'an 710054, China; hezj@nwafu.edu.cn (Z.H.); yanwei.lu@chd.edu.cn (Y.L.)
[2] Key Laboratory of Subsurface Hydrology and Ecological Effect in Arid Region of the Ministry of Education, Chang'an University, Xi'an 710054, China
[3] Key Laboratory of Eco-Hydrology and Water Security in Arid and Semi-Arid Regions of Ministry of Water Resources, Chang'an University, Xi'an 710054, China
[4] Faculty of Modern Agricultural Engineering, Kunming University of Science and Technology, Kunming 650500, China; liangjp@nwafu.edu.cn (Q.Y.); 202111501142@stu.just.edu.cn (C.L.); 202111501132@stu.kust.edu.cn (D.W.)
[5] Yunnan Provincial Field Scientific Observation and Research Station on Water-Soil-Crop System in Seasonal Arid Region, Kunming University of Science and Technology, Kunming 650500, China
* Correspondence: liangjpxaut@163.com
† These authors contributed equally to this work.

Abstract: Water scarcity poses a formidable challenge to agricultural productivity in arid regions, and water retention agents offer promising potential in this regard. Therefore, this study proposes developing and preparing polymers with water retention properties using waste green algae as raw material to explore the effectiveness of enhanced water infiltration and reduce evaporation at different use levels (0%, 0.15%, 0.30%, 0.45% and 0.60%) and maximum mixing depths (10 cm, 20 cm, 30 cm, 40 cm and 50 cm) and determine the optimum management. The results demonstrate that the synthesized polymers exhibited a remarkable swelling rate of 143.6 g/g, along with reusability and excellent temperature stability. The polymer application rate was positively correlated with infiltration duration, with an increase from 161 min to 750 min as the application rate rose from 0% to 0.60%. Concurrently, cumulative infiltration increased from 22.6 cm to 31.1 cm, showcasing the benefits of the polymer in enhancing water retention. Intriguingly, cumulative evapotranspiration initially decreased and then increased with increasing polymer application rates. Moreover, increasing the maximum mixing depth from 10 to 50 cm while maintaining the 0.3% application rate increased the cumulative infiltration (from 22.6 cm to 31.1 cm) and infiltration rate (from 0.03 cm/min to 0.08 cm/min) while decreasing the cumulative evaporation (from 44.4 mm to 31.7 mm). Considering the cumulative infiltration, infiltration rate and evapotranspiration characteristics, an optimized polymer application rate of 0.27% at a mixing depth of 0–50 cm was recommended for efficient soil moisture management. This study highlights the potential of green algae-derived biodegradable polymers as a win–win strategy for achieving waste alleviation of water scarcity in drylands, particularly for maize and wheat cultivation in northern China.

Keywords: waste green algae; swelling rate; application rate; mixing depth; infiltration; evapotranspiration

check for updates

Citation: He, Z.; Liang, J.; Lu, Y.; Yang, Q.; Lu, C.; Wu, D. Enhanced Soil Moisture Management Using Waste Green Algae-Derived Polymers: Optimization of Application Rate and Mixing Depth. *Agronomy* **2023**, *13*, 2335. https://doi.org/10.3390/agronomy13092335

Received: 12 August 2023
Revised: 1 September 2023
Accepted: 5 September 2023
Published: 7 September 2023

Copyright: © 2023 by the authors. Licensee MDPI, Basel, Switzerland. This article is an open access article distributed under the terms and conditions of the Creative Commons Attribution (CC BY) license (https://creativecommons.org/licenses/by/4.0/).

1. Introduction

The growing global population and escalating water scarcity have posed formidable challenges for nations, particularly those inhabiting arid and semiarid regions, to safeguard water sources while ensuring food security [1]. Currently, approximately one-third of the world's agricultural land is adversely affected by water scarcity, resulting in substantial

losses of around 100 million tons of grain production annually [2]. In light of these challenges, enhancing water use efficiency (WUE) emerges as a pivotal strategy that offers multifaceted benefits, including improved water availability, enhanced crop yields, improved crop quality, and ultimately, global food security [3,4]. Thus, the implementation of suitable technical and management measures aimed at optimizing WUE is imperative in attaining sustainable development goals on a global scale.

Among a series of methods for improving WUE, the application of superabsorbent polymers (SAPs), which are known for their special water absorption and retention properties, in soil is considered an effective practical method for increasing yield and WUE [1,3]. SAPs are an innovative class of polymeric chemical materials, characterized by a high density of hydrophilic and cationic binding groups. When exposed to water, SAP undergo rapid swelling, forming insoluble gels that establish a robust three-dimensional network structure, enabling them to effectively retain significant amounts of water. Extensive reports indicated their remarkable water absorption capacity, ranging from 400 to 1600 times their original weight [1,5]. When incorporated into the soil, SAPs promptly absorbed water from rainfall or irrigation, functioning as reservoirs and releasing stored water to plants as soon as the surrounding soil near the root zone begins to desiccate [6,7]. This process significantly enhanced the plant's capacity for water absorption and utilization, facilitating the maintenance of optimal osmotic balance, thus ensuring proper plant growth and development and achieving high yields [8–10]. Generally, the effectiveness of SAPs in preserving soil moisture is contingent upon two fundamental factors: the swelling rate and the water absorption capacity [11,12]. A higher swelling rate and water absorption capacity empowers the SAPs to swiftly acquire water from rainfall or irrigation, thus effectively reducing runoff and evaporation losses while allowing the agent to store and maintain larger quantities of water within its structure. Therefore, investigations focusing on swelling rate and water absorption capacity are essential for studying the performance of SAPs.

In arid/semiarid areas, the soil infiltration rate plays a crucial role in determining the partitioning of rainfall and irrigation water between soil moisture and runoff [13,14]. Moreover, the major pathway of water loss from the soil system is physical evaporation when evapotranspiration by grasses and plants is excluded [15]. Therefore, in practical applications of SAPs, their effects on soil water infiltration and evaporation characteristics are key parameters in determining the final water retention performance [16]. However, the existing literature on the role of SAPs in infiltration has reported conflicting findings [17,18]. Zhao et al. [19] demonstrated that the average infiltration rate decreased with increasing SAP concentration, mainly due to the swelling of SAPs after sufficient water uptake, forming clumps that block soil pores and impede water migration. Albalasmeh et al. [3] indicated that infiltration rates were increased with increasing hydrogel concentration due to the high water-absorbing capacity of the hydrogel. On the other hand, when the SAP was applied in layers, it increased horizontal water infiltration while limiting vertical water infiltration, and increased the infiltration capacity of soil [17,20]. Consequently, this lack of consistent results may be due to both the amount and placement of SAPs in the soil [21,22]. Moreover, an excessive application of SAPs in the soil would strongly impede the infiltration of water, in some cases even causing complete blockage of water infiltration, which can have terrible consequences in real-world settings [16,19]. However, soil–SAP mixed layers designed would reduce the evaporation of water from the underlying soil as well as inhibit the evaporation of water from deeper layers, ultimately increasing water content in the plant rhizosphere [23]. In conclusion, the judicious selection of SAP application location also played a transformative role in its effectiveness. Hence, in practical applications, it is crucial to consider the amount and placement of the SAP on its performance and achieve desired outcomes.

Most of the commercially available superabsorbents are petroleum-based synthetic polymers, characterized by high production costs and limited environmental friendliness [24]. As a result, due to notable advantages such as renewability, biodegradability, biocompatibility, cost-effectiveness, and non-toxicity, the exploration of natural polymeric

materials, including cellulose, starch, alginate, and chitosan, for the synthesis and design of hybrid superabsorbents has gained significant attention [25,26]. In recent years, the rapid development of agriculture and related industries has led to the generation of substantial amounts of wastewater with high levels of nitrogen, phosphorus, and potassium, triggering issues such as water blooms [27,28]. Historically, green algae salvaged from floodplains have been either landfilled or considered low-value, resulting in significant resource waste. Therefore, the utilization of green algae as a soil amendment material to enhance soil moisture offers a promising solution to address both green algae management and water stress in dryland crop cultivation. However, there is a lack of comprehensive research on the properties of water-holding agents derived from green algae. Hence, this study aims to (i) investigate the swelling characteristics of a polymer derived from green algae, (ii) assess the impact of different application rates and mixing depths on infiltration and evaporation, and (iii) determine optimal green algal polymer management strategies to promote infiltration and inhibit evaporation. Our findings can inform the development of sustainable strategies for utilizing green algae as a valuable resource in soil management practices.

2. Materials and Methods

2.1. Materials

The main raw material for this study was green algae from Dianchi Lake (24°50′ N, 102°40′ E), a place heavily troubled by water eutrophication [29]. Other utilized reagents (alginate lyase, green algae polysaccharide lyase, sodium hydroxide, nitric acid, ethanol, potassium persulfate, bentonite acid-leached, acrylic acid, N,N'methylenebisacrylamide (MBA), green algae polysaccharide-degrading bacteria and anti-freezer) were all of analytical grade.

2.2. Synthesis of the Green Algae Polymers

A series of different proportions of samples were prepared through the following steps. The fresh green algae salvaged from Dianchi Lake was cleaned and dried, then crushed and sieved with a grinder. The dried powder of green algae was poured into a lyase cell for hydrolysis, followed by centrifugation and membrane separation. Further treatment with alkali and nitric acid–ethanol allowed for the isolation of green alga cellulose, which was subsequently processed through centrifugation, grinding, sieving, and washing to obtain green algae extract. The extract was then combined with potassium persulfate, acid-leached bentonite, and deionized water, and the resulting mixture was subjected to microwave heating, yielding a green algae fiber mixture. The fiber mixture was then modified through neutralization with acrylic acid and sodium hydroxide in an ice-water bath, incorporating MBA as a cross-linking agent to obtain a reaction solution. Addition of a carbon base material inoculated with degradation bacteria and antifreeze agents, followed by microwave heating, led to the formation of a gel-state primary product. This product was subsequently washed, dried, and ground to obtain the final green algae polymer (Figure 1).



Figure 1. Synthesized green alga polymer.

2.3. Green Algae Polymer Performance Testing

2.3.1. Swelling Behavior and Reuse Performance Test

A tea bag method was employed to measure the swelling behavior of the polymer samples [30,31]. The specific process is shown in Figure 2. First, 0.1 g of dried green algae polymer powder was placed in a 100-mesh tea bag. Then, the tea bag was immersed in 100 mL of deionized water solution [31]. Subsequently, at specific times of 10, 20, 30, 50, 70, 120, 180, 240, 360, and 1440 min, the tea bag was removed and hung to exclude unabsorbed water [32]. When the dripping ceased (Figure 2c), the swelling rate (SR) was determined by employing Equation (1):

$$SR_t = (W_t - W_d)/W_d \quad (1)$$

where SR_t represents the swelling rate at the time t, W_t is the weight of the swollen green algae polymer at the time t, and W_d is the initial dry weight of the polymer.

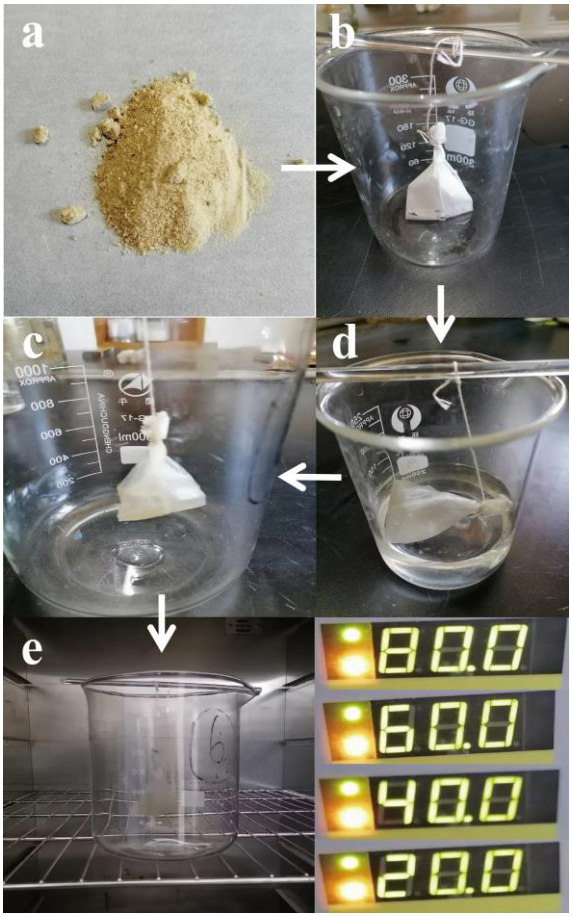

Figure 2. Swelling behavior and water retention capacity testing of green algae polymers. (**a**) green alga polymer. (**b**–**d**) show the polymer's state before, during, and after swelling in tea bag, respectively. (**e**) is fully swollen polymers dried at different temperatures.The arrows denote the sequential experimental stages of the polymer, from swelling to drying.

When SR remains constant and unchanging over a specific period, the polymer is considered to be fully swollen. The fully swollen polymer was then dried in a 60 °C oven until a constant weight was attained [33]. This "swelling–drying" process was repeated eight times as the reuse performance test [32,34]. The swelling rate was recorded after each cycle.

2.3.2. Water Retention Capacity

Based on previous studies, the water retention capacity was determined using the heating test [33,35]. Specifically, a certain amount of fully swollen polymer was placed in a beaker and dried in an oven at different temperatures (Figure 2e). Subsequently, the samples were periodically weighed at specified time intervals. In this study, a total of 50 g of the fully swollen polymer was placed in a beaker and subjected to drying in an oven at temperatures of 20 °C, 40 °C, 60 °C, and 80 °C [26,36]. The weight of the green algae polymer samples was recorded at specific times of 10, 20, 30, 50, 80, 120, 240, 360 and 480 min. The water retention capacity at different temperatures was calculated using Equation (2) [32,33]:

$$W_T\ (\%) = W_t/W_0 \cdot 100 \quad (2)$$

where W_T represents the water retention rate per gram of swelled sample, W_t is the weight of the swollen green algae polymer at time t, and W_0 is the mass of the saturated swollen gel.

2.4. Soil Infiltration and Evaporation with Green Algae Polymer

The experiment consisted of two parts, focusing on different amounts of green algae polymer and varying mixing depths. In the first part, 0% (CK), 0.15%, 0.30%, 0.45% and 0.60% polymers were uniformly distributed in the 0–50 cm soil layer. In the second part, 0.9 g of green algae polymer (equivalent to 0.30% of the polymer uniformly mixed in 0–50 cm soil layer) was applied in different soil layers, including 0–10, 0–20, 0–30, 0–40, and 0–50 cm, corresponding to maximum mixing depths of 10 cm, 20 cm, 30 cm, 40 cm, and 50 cm, respectively. Each treatment was repeated three times to ensure reliability and consistency. The soil used for the experiment was a clay loam, consisting of 22.8% clay, 40.7% silt and 36.5% sand. The soil bulk density was 1.32 g/cm^3, measured using a ring knife. The soil pH was 6.72 and the soil moisture content curve is shown in Figure 3.

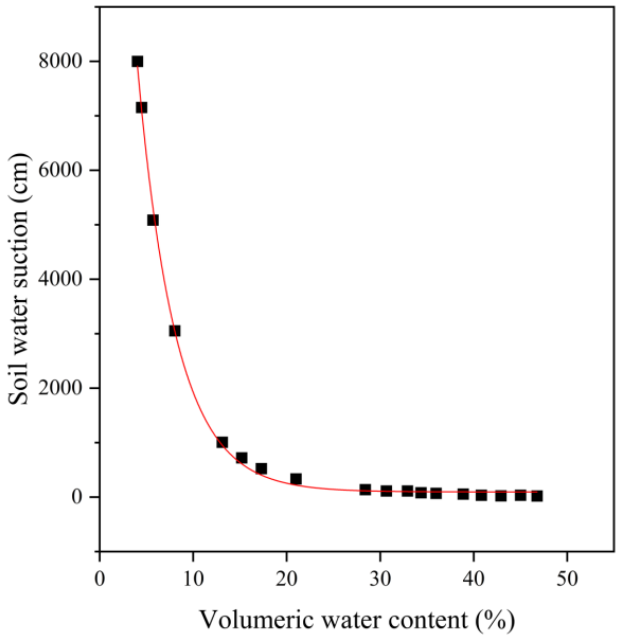

Figure 3. Moisture content curve of the soil used in the test.

2.4.1. Soil Water Infiltration

First, the polymer and soil were thoroughly mixed according to the experimental design. Then, the columns were carefully filled by successively filling and compacting 5 cm of the soil–polymer mixture [37]. The soil columns were filled to a height of 50 cm. To mitigate surface effects resulting from irrigation and prevent the escape of fine particles, filter paper was positioned both at the top and bottom of the soil layer [37]. Infiltration experiments were conducted under constant head conditions, maintaining the water level

at 3.5 cm above the soil surface. A stopwatch was used to record the time intervals during the infiltration process. Observations were made at 1, 3, 5, 7, 10, 15, 20, 30, and 60 min after wetting initiation, followed by 30 min intervals until the wetting front reached a depth of 50 cm. Additional recordings of penetration times were made when wetting front of 20 cm and 50 cm was reached. The cumulative infiltration was also monitored using the Marriott bottle scale.

2.4.2. Soil Water Evapotranspiration

The soil water evapotranspiration test was mainly composed of infrared lamp and infiltration-completed soil columns. After the soil infiltration process, firstly, the soil column was transferred to a stabilized room environment (temperature 20 ± 2 °C, relative humidity 50%), then the filter paper was removed from the surface of the soil column (no covering or mulching on the surface) (Figure 4). Next, an infrared light source rated at 275 W was installed 25 cm above the soil column to provide heating for soil water evapotranspiration [21,38]. The light source was turned on throughout the day and night to ensure continuous evaporation [39]. The weight method was employed to measure the evaporation from the soil columns at specific intervals, including 1, 2, 3, 4, 6, 8, 10, 12, 15, 18, 21, 24, 36, and 48 h after the initiation of evaporation [38,39].

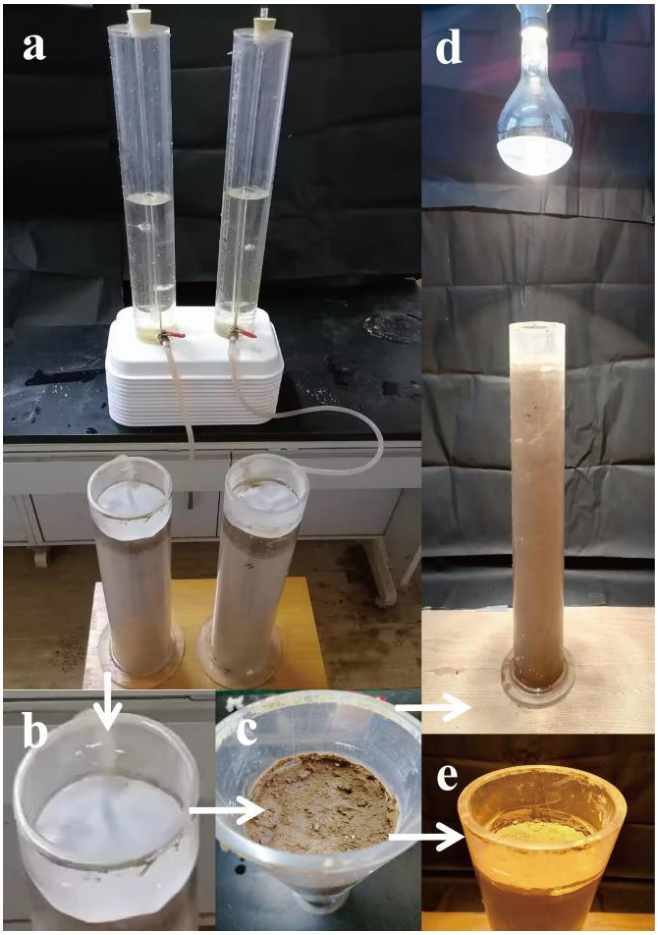

Figure 4. Soil water infiltration and evapotranspiration testing of green algal polymer-mixed soils. (**a**) is overall view of the soil water infiltration experiment. (**b**,**c**) show the soil column covered with filter paper during infiltration and filter paper removed before evapotranspiration experiments, respectively. (**d**,**e**) are overall and localized views of the soil water evapotranspiration experiment, respectively. The arrows denote the sequential experimental stages from the infiltration to the evapotranspiration experiments.

2.5. Infiltration Models, Evaporation Models and Evaluation Indices

2.5.1. Wetting Front Propulsion Model

The advancement of the wetting front during the infiltration process can be accurately described by a power function [40]. To estimate the depth of the wetting front, the following equation is employed:

$$F_z = At^B \tag{3}$$

where F_z is the depth of the wetting front (cm) and A and B are fitting parameters.

2.5.2. Cumulative Infiltration Model

Cumulative infiltration was quantified utilizing well-established models, including the Lewis equation, the Philip infiltration model, and the Horton infiltration model [37,41]. The formulas are as follows:

1. Lewis equation:

$$I = Kt^{\alpha} \tag{4}$$

where I represents the cumulative infiltration (cm), K and α are fitting parameters, and t denotes the time of infiltration (min).

2. Philip infiltration model:

$$I = St^{0.5} \tag{5}$$

where S is the sorptivity ($cm/min^{0.5}$).

3. Horton infiltration model:

$$I = at + (b - a)(1 - e^{-ct})/c \tag{6}$$

In this equation, a and b indicate the presumed final and initial infiltration rates (cm/min), respectively, and c represents an empirical constant.

2.5.3. Evaporation Model

To investigate the impact of different amounts of green algae polymer and varying mixing depths on soil evaporation, both the Black evaporation model and Rose evaporation model were utilized [38].

(1) Black evaporation model:

$$E = F + Bt_0{}^{0.5} \tag{7}$$

where E represents the cumulative evaporation amount (g), t_0 is the time evaporation (h). F and B are fitting parameters.

(2) Rose evaporation model:

$$E = Ct_0 + Dt_0{}^{0.5} \tag{8}$$

where E represents the cumulative evaporation amount (g), t_0 is the evaporation calendar time (h), C represents the stable evaporation parameter, and D represents the moisture diffusion parameter.

2.5.4. Evaluating Indices of Models

To evaluate the model's effectiveness, various statistical criteria were employed, including mean absolute error (MAE), relative root mean square error (RRMSE), coefficient of residual mass (CRM), and coefficient of efficiency (CE). The formulas are as follows:

$$\mathrm{MAE} = \frac{\sum_{i=1}^{n} |Y_{iobis} - Y_{isim}|}{n} \tag{9}$$

$$\mathrm{RRMSE} = \sqrt{n^{-1} \sum_{i=1}^{n} (Y_{iobis} - Y_{isim})^2} \tag{10}$$

$$\mathrm{CRM} = \frac{\sum_{i=1}^{n}(Y_{iobis} - Y_{isim}) \cdot 100}{\sum_{i=1}^{n} Y_{iobis}} \tag{11}$$

$$\mathrm{CE} = 1 - \frac{\sum_{i=1}^{n}(Y_{iobis} - Y_{isim})^2}{\sum_{i=1}^{n}(Y_{iobis} - Y_{mean})^2} \tag{12}$$

where Y_{iobs} is the ith measured value, Y_{isim} is the ith simulated value, Y_{mean} denotes the average of the measured values, and n represents the total number of data points.

2.6. Comprehensive Evaluation

A comprehensive evaluation of the infiltration and evapotranspiration behavior under different treatments was conducted using TOPSIS to obtain the best management practices for green algal polymers. Based on the number of evaluation objects and indicators, a decision matrix is formed and normalized using Equation (13):

$$n_{ij} = a_{ij} \Big/ \sqrt{\sum_{i=1}^{m} {a_{ij}}^2} \tag{13}$$

where a_{ij} represents the jth indicator in the ith evaluation objects.

The v_{ij} is calculated as follows:

$$v_{ij} = w_i \times n_{ij} \tag{14}$$

where w_i is the weight, calculated by the entropy weight method [42].

The positive ideal solution values (A^+) and negative ideal solution values (A^-) are determined by Equations (15) and (16):

$$A^+ = \{\max v_{ij}\} \rightarrow A^+ = \{{v_1}^+, {v_2}^+, \cdots, {v_j}^+\} \tag{15}$$

$$A^- = \{\min v_{ij}\} \rightarrow A^- = \{{v_1}^-, {v_2}^-, \cdots, {v_j}^-\} \tag{16}$$

With the help of Equations (17) and (18), the Euclidian distance between A^+ and A^- is calculated. The closeness index (CI) is derived from Equation (19).

$${D_i}^+ = \sqrt{\sum_{j=1}^{n} ({v_j}^+ - v_{ij})^2} \tag{17}$$

$${D_i}^- = \sqrt{\sum_{j=1}^{n} ({v_j}^- - v_{ij})^2} \tag{18}$$

The closeness index (CI) is given by Equation (18). The higher the CI, better the object is relative to others.

$$CI_i = {D_i}^- / \left({D_i}^+ + {D_i}^-\right),\ i = 1, 2, \ldots, 10. \tag{19}$$

2.7. Statistical Analysis

Statistical analysis of the experimental data was conducted using SPSS software (version 26) and MATLAB 2020a program (MathWorks, Natick, MA, USA). Differences were deemed statistically significant at a significance level of 0.05. The visualization of data was performed using Origin 2023a (OriginLab, Northampton, MA, USA).

3. Results

3.1. Swelling Performance

The swelling time exerted a significant impact on the swelling rate of the green algae polymer, as illustrated in Figure 5a ($p < 0.05$). Consistent with expectations, upon contact with water, the green algae polymer promptly absorbed water, leading to rapid expansion and an increasing swelling rate with prolonged contact time. Initially, the swelling rate experienced a steep rise, culminating in a swelling rate of 100.3 g/g within the initial 10 min. However, the rate of increase in swelling slowed down over time. Following exposure durations of 20 min, 30 min, 50 min, and 70 min, the corresponding swelling rates were measured to be 123.8 g/g, 129.5 g/g, 133.9 g/g and 137.4 g/g, respectively. Accordingly, the swelling rate increased by only 12.5 g/g, 5.7 g/g, 4.4 g/g and 3.5 g/g during 10–20 min, 20–30 min, 30–50 min and 50–70 min, respectively. Beyond 120 min of contact time, the effect of swelling time on swelling rate became statistically insignificant, indicating that full swelling had been achieved. The full swelling rate of the green algae polymer was as high as 143.6 g/g, showing its excellent water absorption capacity and potential as a water retention agent, expanding the application of green algae in agriculture in arid areas.

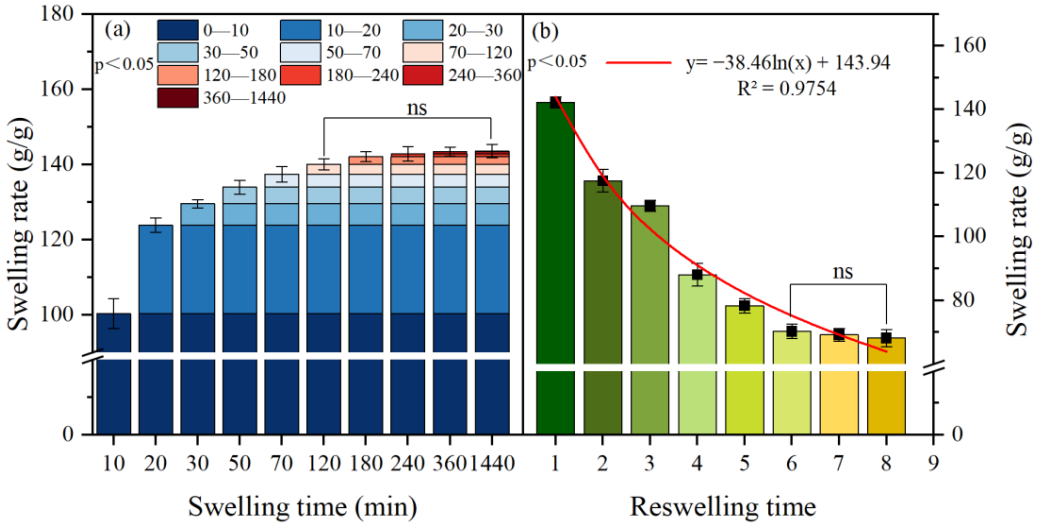

Figure 5. Swelling rate of green algae polymer in different swelling time and reswelling time in fresh water. Different colors in (**a**) represent the increase in swelling rate at different time periods. $p > 0.05$ and $p < 0.05$ indicate non-significant and significant effects of (**a**) swelling time and (**b**) reswelling time on swelling rate at the $p = 0.05$ level, respectively. ns indicates insignificant at the $p = 0.05$ level.

The reswelling time has been found to significantly impact the swelling rate of polymer. Throughout cycles 1, 2, 3, 4, and 5, the polymer exhibited full swelling rates of 142.2 g/g, 117.6 g/g, 109.7 g/g and 88.1 g/g, respectively, owing to the decomposition of polymer in water. Although the swelling rate of the polymer diminished with increasing number of swelling cycles, the downward trend exhibited a deceleration effect. After undergoing five swelling cycles, the swelling rate still reached 55% of the initial value. Notably, during cycles 6, 7, and 8, the polymer demonstrated consistent swelling rates ranging from 70.2 g/g to 68.1 g/g, with no significant differences observed between them, indicative of a certain degree of structural stability. Additionally, the swelling characteristics of polymer under repeated usage were effectively described by a logarithmic equation, reaffirming the sustained favorable swelling ability of the polymers. This highlights its long service life and positions it as an economically viable material for repetitive water absorption applications.

3.2. Water Retention Capacity

Green algae polymer's water retention capacity reveals a substantial reduction with rising temperatures and elapsed time (Figure 6). Elevated temperatures led to more pronounced water retention curves, with the optimum water retention observed at 20 °C.

At 10 min, the water retention capacity was 89.6%, exceeding those at 35 °C, 60 °C, and 80 °C by 5.1%, 9.1%, and 18.4%, respectively. The difference was more pronounced at 240 min, with the water retention capacity surpassing that at 40 °C, 60° C, and 80 °C by 14.3%, 41.4%, and 44.6%, respectively. At 480 min, the capacity decreased to 29.2%, indicating reduced performance over an extended duration. At 40 °C, the polymer experienced significant moisture loss, resulting in a water retention capacity of only 1.6% after 480 min. Moreover, at 60 °C and 80 °C, the water retention capacity declined rapidly over time, with both temperatures losing their water retention efficacy after 360 and 240 min, respectively. Overall, although green algal polymer demonstrated excellent water retention properties at low temperatures, the negative impact of high temperatures on the water retention capacity must be taken into account in practical applications. Thus, prudent evaluation of specific temperature and time conditions is indispensable when employing green algae polymer to ensure optimal utility.

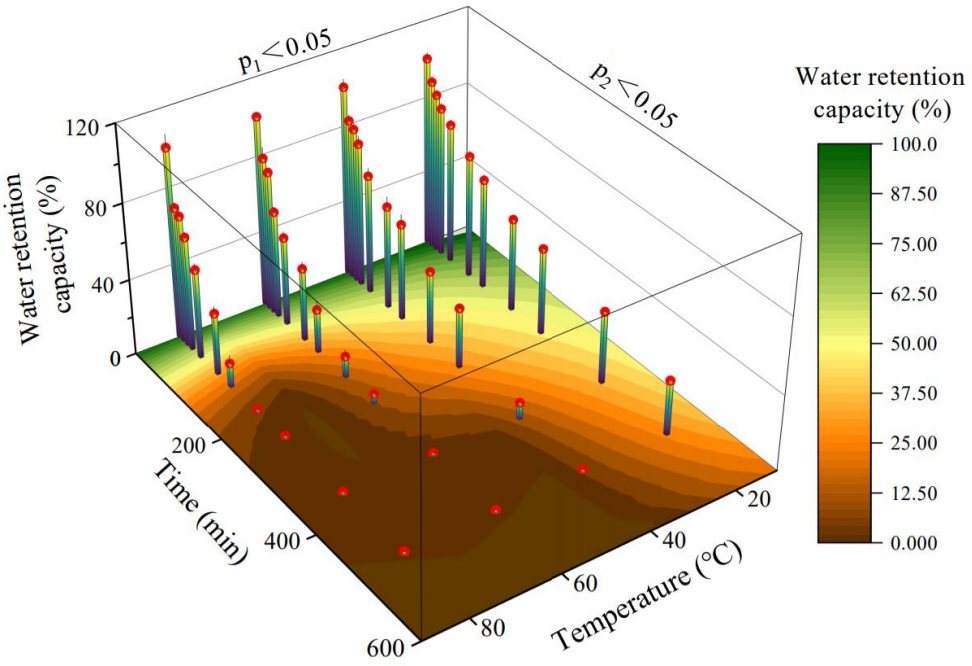

Figure 6. Water retention capacity of green algae polymer at different temperatures. $p > 0.05$ and $p < 0.05$ indicate non-significant and significant effects of time (p_1) and temperature (p_2) on water retention capacity at the $p = 0.05$ level, respectively.

3.3. Soil Water Infiltration

3.3.1. Wetting Front

The migration process of the wetting front under varying polymer application rates is depicted in Figure 7a. Initially, the wetting front experienced a rapid decrease in velocity for different polymer application rates, gradually slowing down as time elapsed. This phenomenon could be attributed to the dryness of the soil surface during the initial infiltration phase, leading to a substantial water potential gradient and unsaturated degree on the wetting front's surface, resulting in a fast infiltration rate. No significant difference was observed among different treatments within the first 30 min. However, over time, differences in the time taken for the wetting front to reach the same depth were increasing between treatments. For instance, when the wetting fronts reached a depth of 20 cm, the infiltration time for the CK, 0.15%, 0.30%, 0.45%, and 0.60% treatments was 30 min, 67 min, 79 min, 70 min and 120 min, respectively (Figure 7c). Significantly less time was consumed by the CK treatment compared to other treatments ($p < 0.05$), while the 0.60% application rate required significantly more time than the other treatments. Furthermore, there was no statistically significant difference between 0.15%, 0.30%, and 0.45% treatments. The difference became more pronounced when the wetting front reached 50 cm. At this time,

the time consumption for the CK, 0.15%, 0.30%, 0.45%, and 0.60% treatments amounted to 161 min, 232 min, 360 min, 448 min and 750 min, respectively, with significant differences among the different treatments (Figure 7e). These observations confirmed that the polymer decelerated the migration of the wetting front, and the larger the application rate, the longer the infiltration duration and the more pronounced the reduction effect.

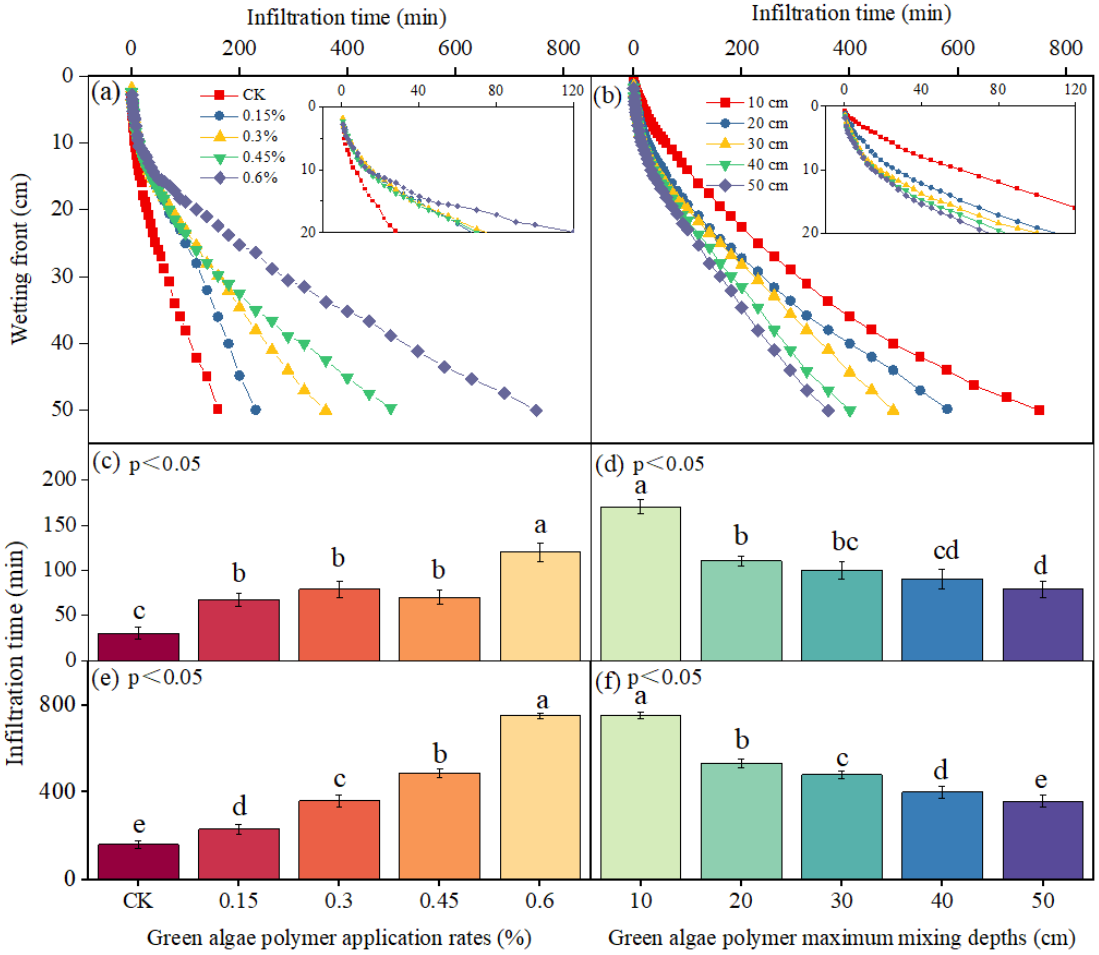

Figure 7. Effects of different polymer application rates and depths on wetting front. (**a**) Characterization of the wetting front with time under different polymer application rates. (**b**) Characterization of the wetting front with time under different maximum mixing depths. (**c**) Elapsed time for the wetting front to reach 20 cm under different polymer application rates. (**d**) Elapsed time for the wetting front to reach 20 cm under different maximum mixing depths. (**e**) Elapsed time for the wetting front to reach 50 cm under different polymer application rates. (**f**) Elapsed time for the wetting front to reach 50 cm under different maximum mixing depths. Different letters on the bars indicate significant differences at $p = 0.05$ level.

The wetting front migration exhibited a general decreasing trend with different maximum mixing depths, in line with varying polymer application rates (Figure 7b). During the initial stage, the wetting front migration remained at a relatively high level, but as time elapsed, it gradually stabilized. Upon reaching a depth of 20 cm, the infiltration time for treatments with maximum mixing depths of 10 cm, 20 cm, 30 cm, 40 cm and 50 cm was 170 min, 110 min, 100 min, 90 min and 79 min, respectively (Figure 7d). The treatment with a maximum mining depth of 10 cm exhibited significantly longer infiltration time compared to other treatments. At the end of infiltration, the infiltration time decreased with increasing maximum mixing depths, with significant differences among the different treatments (Figure 7f). Overall, under the same polymer application rate, larger maximum mixing depths favored the migration of the wetting front.

3.3.2. Cumulative Infiltration

Cumulative infiltrations all tended to increase with time, and different polymer application rates had a significant effect on cumulative infiltration (Figure 8a). As infiltration progressed, the differences in cumulative infiltration between various polymer application rates exhibited a pattern of initially widening, then narrowing, and eventually widening again. At the beginning of infiltration, high polymer application rates, particularly the 0.60% application rate, led to a more rapid increase in cumulative infiltration. Specifically, the 0.60% and 0.45% treatments demonstrated notably higher average infiltration rates than other treatments during the first 5 min (Figure 8c). However, this was not sustainable. As time progressed, the cumulative infiltration of the low-application-rate treatments gradually exceeded that of the high-application-rate treatments. Notably, the low application rate resulted in a shorter infiltration duration, while the high-application-rate treatments had longer infiltration process, resulting in ongoing cumulative infiltration. At the end of infiltration, the cumulative infiltration for CK, 0.15%, 0.30%, 0.45%, and 0.60% treatments was 22.6 cm, 24.8 cm, 28.2 cm, 29.2 cm and 31.1 cm, respectively. It was clear that polymer application significantly increased cumulative infiltration, with the higher application rates having a greater effect. However, due to the long infiltration duration at high application rates, the average infiltration rate decreased significantly at the end of the infiltration as the amount of polymer increased (Figure 8e). In conclusion, polymer application increased the cumulative infiltration, but decreased the average infiltration rate throughout the infiltration phase.

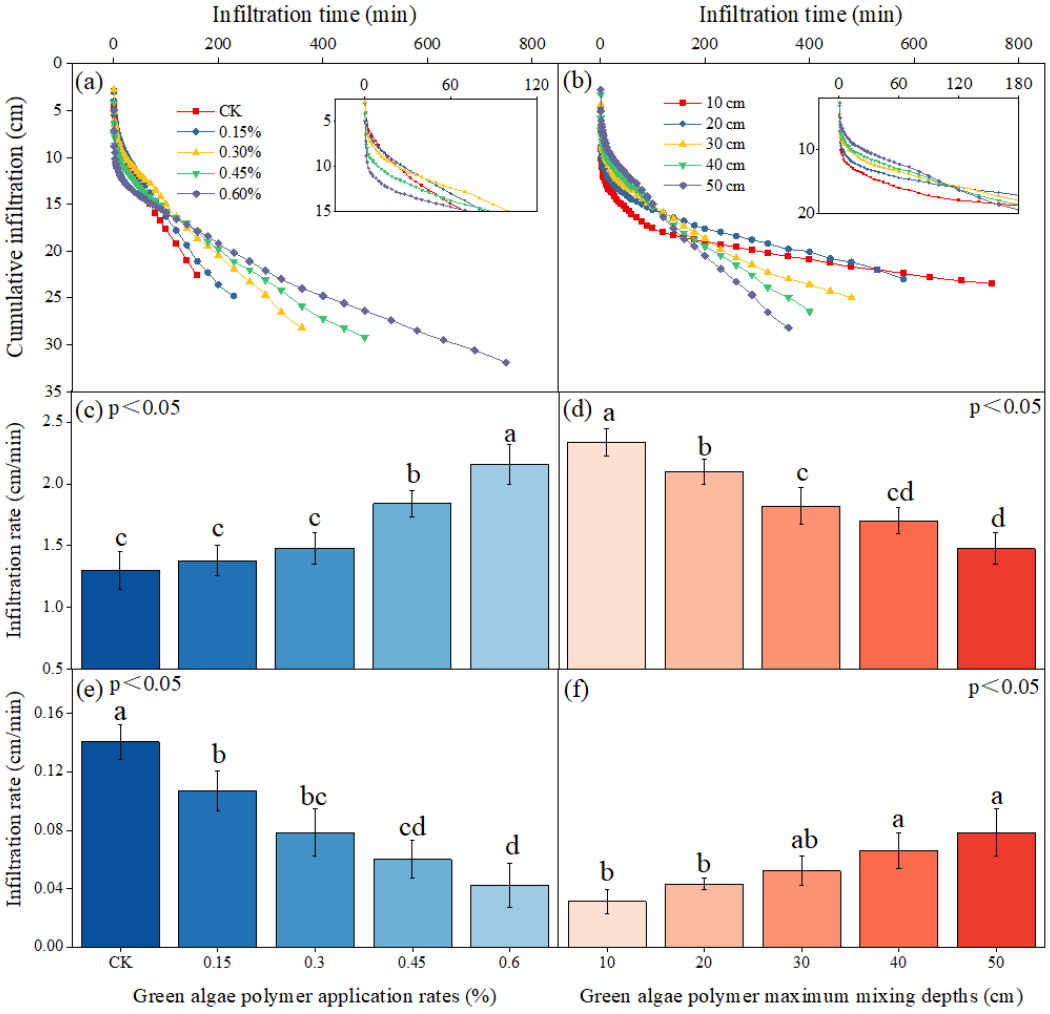

Figure 8. Effects of different polymer application rates and depths on cumulative infiltration. (**a**) Characterization of cumulative infiltration with time under different polymer application rates. (**b**) Characterization

of cumulative infiltration with time under different maximum mixing depths. (**c**) Average infiltration rate in the first 5 min at different polymer application rates. (**d**) Average infiltration rate at the end of infiltration at different polymer application rates. (**e**) Average infiltration rate in the first 5 min at different polymer application rates. (**f**) Average infiltration rate at the end of infiltration at different maximum mixing depths. Different letters on the bars indicate significant differences at $p = 0.05$ level.

Cumulative infiltration was found to be significantly influenced by maximum mixing depths (Figure 8b). Similar to the observed changes in cumulative infiltration with varying application rates, the differences in cumulative infiltration between treatments at different mixing depths exhibited a pattern of initial widening, followed by narrowing, and then widening again. At the commencement of infiltration, shallower depths corresponded to greater cumulative infiltration and, consequently, higher average infiltration rates. During the initial 5 min, the infiltration rates for the maximum mixing depths of 10 cm, 20 cm, 30 cm, 40 cm, and 50 cm were 2.3 cm/min, 2.1 cm/min, 1.8 cm/min, 1.7 cm/min and 1.5 cm/min (Figure 8d). However, as time advanced, the cumulative infiltration of the treatments with deeper mixing depths gradually exceeded that of the shallower treatments. At the end of infiltration, the cumulative infiltration for the treatments was 23.5 cm, 23.0 cm, 25.0 cm, 26.5 cm and 28.2 cm. These results highlight that greater maximum mixing depths favorably impact the cumulative infiltration. Furthermore, deeper mixing depths also increased the average infiltration rate due to the shorter infiltration duration.

3.3.3. Infiltration Model

The fitting parameters of the wetting front propulsion model are presented in Table 1. During the model evaluation, the optimal values for MAE, RRRMSE, CRM, and CE were 0, 0, 0, and 1, respectively. A closer proximity to these optimal values indicates a smaller discrepancy between the simulated and measured values, implying a better model performance. In this study, the MAE, RMSE, CRM, and CE values for different polymer application rates ranged from 0.423 to 1.055, 0.021 to 0.10, 0.002 to 0.023 and 0.979 to 0.999, respectively. Similarly, for various maximum mixing depths, the MAE, RMSE, CRM, and CE values also fell within the ranges of 0.270 to 1.01, 0.019 to 0.063, −0.001 to 0.011 and 0.992 to 0.999, respectively. Obviously, the simulated migration of the wetting front demonstrated good agreement with the observed values, indicating that the power function performed well in simulating the transport characteristics of wetting front with polymer addition.

Table 1. Fitting parameters of wetting front propulsion model and cumulative infiltration model.

			Application Rate (%)					Maximum Mixing Depths (cm)				
		Treatments	**CK**	**0.15**	**0.3**	**0.45**	**0.6**	**10**	**20**	**30**	**40**	**50**
Wetting front propulsion model		A	3.611	1.649	2.032	2.975	2.756	0.789	1.693	2.002	2.094	2.184
		B	0.511	0.611	0.543	0.453	0.429	0.632	0.528	0.511	0.522	0.525
		MAE	0.423	1.522	1.191	0.35	1.055	0.409	0.270	0.911	1.010	0.881
		RRMSE	0.026	0.105	0.079	0.021	0.061	0.034	0.019	0.063	0.063	0.054
		CRM	0.004	0.023	0.014	0.002	0.009	−0.001	0.002	0.009	0.011	0.010
		CE	0.998	0.979	0.988	0.999	0.992	0.999	0.999	0.993	0.992	0.994
Cumulative infiltration model	Lewis	K	3.347	3.160	3.697	4.891	6.067	8.636	7.631	5.646	4.812	3.697
		α	0.361	0.366	0.322	0.273	0.234	0.150	0.162	0.231	0.267	0.322
		MAE	0.511	0.879	0.989	1.149	1.284	0.303	0.472	0.734	0.933	0.989
		RRMSE	0.057	0.084	0.094	0.092	0.090	0.034	0.042	0.061	0.081	0.094
		CRM	0.006	0.010	0.009	0.007	0.006	−0.001	0.000	0.003	0.005	0.009
		CE	0.984	0.969	0.957	0.953	0.947	0.984	0.977	0.973	0.960	0.957
	Philip	S	1.878	1.723	1.56	1.489	1.338	1.192	1.234	1.385	1.489	1.56
		MAE	0.901	1.238	1.624	2.262	2.986	3.085	2.796	2.185	1.986	1.624
		RRMSE	0.098	0.123	0.153	0.181	0.21	0.224	0.225	0.182	0.173	0.153
		CRM	0.03	0.039	0.052	0.067	0.082	0.087	0.084	0.067	0.061	0.052
		CE	0.953	0.935	0.888	0.815	0.713	0.317	0.345	0.753	0.818	0.888

Table 1. *Cont.*

			Application Rate (%)					Maximum Mixing Depths (cm)				
		Treatments	**CK**	**0.15**	**0.3**	**0.45**	**0.6**	**10**	**20**	**30**	**40**	**50**
Cumulative infiltration model	Horton	a	0.141	0.108	0.083	0.061	0.043	0.031	0.04	0.052	0.066	0.083
		b	6	6	5.6	8.4	10	9.7	9.2	8.8	6.6	5.6
		c	1.075	0.996	0.849	1.003	1.007	0.858	0.945	1.004	0.84	0.849
		MAE	1.154	1.098	1.529	1.81	2.133	2.541	2.4	1.723	1.757	1.529
		RRMSE	0.148	0.136	0.168	0.168	0.177	0.216	0.219	0.177	0.177	0.168
		CRM	0.004	0.003	0.007	0.004	0.004	0.003	0.005	0.004	0.006	0.007
		CE	0.892	0.92	0.865	0.841	0.797	0.363	0.381	0.768	0.81	0.865

To further analyze the effect of polymer use on the water infiltration process, the measured cumulative infiltration data were fitted using Lewis, Philip and Horton models, and the results are shown in Table 1. Within the Philip model, "S" represents the sorptivity, characterizing the soil water infiltration capacity. As the polymer usage increased, the S value gradually decreased, indicating a reduction in soil moisture infiltration capacity with increasing polymer application rates. For different polymer application rates, the MAE, RMSE, CRM, and CE values for the Lewis equation ranged from 0.511 to 1.284, 0.057 to 0.094, 0.006 to 0.01 and 0.947 to 0.984, respectively. Similarly, the corresponding parameters for the Philip model ranged from 0.901 to 2.986, 0.098 to 0.21, 0.030 to 0.082, and 0.713 to 0.953, respectively. Meanwhile, the Horton model exhibited parameters ranging between 1.098 and 2.188, 0.136 and 0.177, 0.003 and 0.007, and 0.797 and 0.920, respectively. Clearly, the statistical indices (MAE, RRMSE, CRM, and CE) of the Lewis equation approach the optimal values, resulting in superior simulation outcomes. Similar trends were also observed for various mixing depths. Evidently, the Lewis equation was more suitable than the Horton or Philip model in simulating cumulative soil infiltration in the presence of polymers, as it more realistically reflected the changes in cumulative soil infiltration over time with polymer addition.

3.4. Soil Cumulative Evaporation

The cumulative evapotranspiration was significantly influenced by both polymer application rate and maximum mixing depth treatments (Figure 9). Over time, all treatments exhibited an increase in cumulative evapotranspiration, with the rate of increase gradually decreasing, consistent with the dehydration process. During the initial stage of evaporation, each treatment displayed a higher soil surface water content, resulting in larger evaporation and consequently higher cumulative evaporation. Specifically, within the first hour, the cumulative evaporation for CK, 0.15%, 0.30%, 0.45%, and 0.60% treatments was 4.8 mm, 5.1 mm, 5.1 mm, 5.5 mm and 5.9 mm, respectively. Similar trends were observed for treatments with different maximum mixing depths. As the evaporation time increased, the surface layer underwent desiccation and the addition of polymer hindered the evaporation of soil moisture, thereby reducing cumulative evaporation. Specifically, the addition of 0.15% and 0.30% polymer led to a significant reduction in evaporation by 12% and 15%, respectively, in evaporation over 48 h of evaporation compared to CK. However, with a further increase in polymer application rate, an increase in cumulative evaporation was observed. At a 0.60% application rate, the maximum cumulative evaporation was even 35% higher than the CK treatment, proving detrimental to soil moisture retention. Furthermore, the evaporation process of soil moisture exhibited higher cumulative evaporation for treatments with smaller maximum mixing depths. After 48 h, the cumulative evaporation for treatments with maximum mixing depths of 10 cm, 20 cm, 30 cm, 40 cm and 50 cm was 44.4 mm, 42.2 mm, 37.4 mm, 36.5 mm and 31.7 mm, respectively. In other words, a uniform distribution of 0.30% polymer over a depth of 0–50 cm was found to be most effective in reducing soil moisture evaporation.

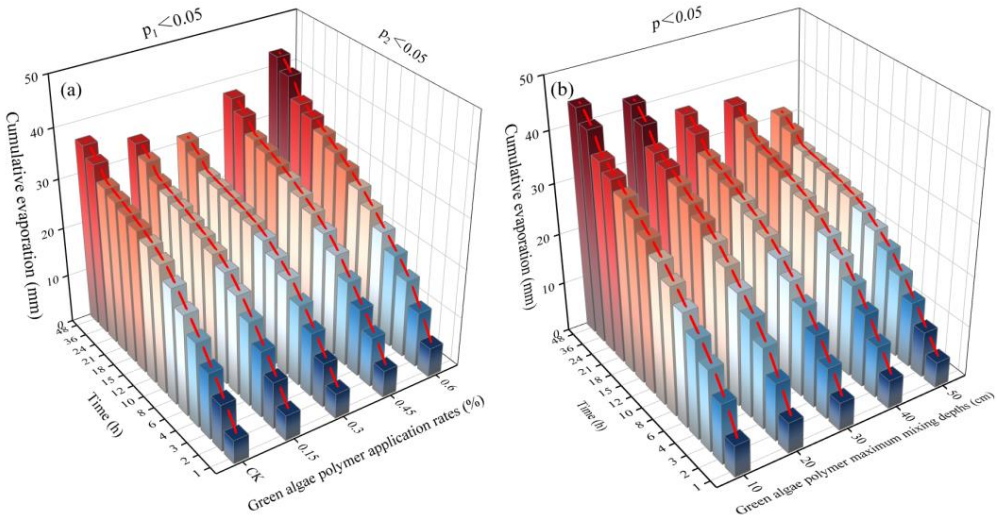

Figure 9. Effects of different polymer application (**a**) rates and (**b**) depths on cumulative evaporation.

Table 2 presents the performance of the Black and Rose models in simulating soil evapotranspiration at different polymer application rates and maximum mixing depths. For the Black evapotranspiration model, the values of MAE, RRMSE, CRM and CE ranged from 2.21 to 2.75, 0.10 to 0.14, 0 and 0.85 to 0.94, respectively, for different polymer application rates, indicating good fitting accuracy of the model. Notably, with an increase in polymer usage, CE demonstrated a gradual increase, implying an improvement in model accuracy. Similarly, the Black model exhibited values of MAE, RMSE, CRM, and CE ranging from 2.23 to 2.70, 0.10 to 0.14, 0 and 0.85 to 0.94, respectively, for different polymer usage, which further affirmed its acceptable fitting accuracy. However, a concern arose with the Rose model as the stable evaporation parameter "C" was found to be negative, contradicting the observed facts and rendering the results of the Rose model unreliable. In summary, the Black model effectively reflected the cumulative soil evaporation over time under polymer addition with good and realistic accuracy.

Table 2. Fitting parameters of evaporation model.

			Application Rate (%)				Maximum Mixing Depths (cm)				
	Treatments	**CK**	**0.15**	**0.3**	**0.45**	**0.6**	**10**	**20**	**30**	**40**	**50**
Black	F	5.89	6.7	6.96	6.06	5.58	5.8	6.45	6.27	7.15	6.96
	B	5.22	4.62	4.2	5.23	6.12	6.29	5.89	5.16	4.94	4.2
	MAE	2.75	2.54	2.56	2.47	2.21	2.23	2.45	2.39	2.7	2.56
	RRMSE	0.13	0.13	0.14	0.12	0.1	0.1	0.11	0.12	0.13	0.14
	CRM	0	0	0	0	0	0	0	0	0	0
	CE	0.88	0.87	0.85	0.9	0.94	0.94	0.92	0.91	0.88	0.85
Rose	C	−0.63	−0.66	−0.67	−0.61	−0.57	−0.58	−0.64	−0.62	−0.7	−0.67
	D	9.69	9.41	9.15	9.67	10.21	10.51	10.56	9.68	10.07	9.15
	MAE	1.21	1.17	1.21	0.96	0.72	0.7	0.8	0.92	1.11	1.21
	RRMSE	0.07	0.06	0.07	0.05	0.04	0.04	0.05	0.05	0.06	0.07
	CRM	−0.01	−0.01	−0.01	−0.01	−0.01	−0.01	−0.01	−0.01	−0.01	−0.01
	CE	0.97	0.97	0.96	0.98	0.99	0.99	0.98	0.98	0.97	0.96

3.5. Optimal Polymer Management Practices Based on Comprehensive TOPSIS Evaluations

Both the polymer application rate and maximum mixing depth influenced the comprehensive evaluation scores (Table 3). As the application rate increased, the score initially rose before declining. The score for the 0.60% treatment was 0.47, lower than the score for CK (0.51), indicating potential negative effects from improper polymer usage. The treatment with 0.30% polymer exhibited the highest score of 0.62, representing the most favorable

overall benefits. Across different maximum mixing depths (10 cm, 20 cm, 30 cm, 40 cm, and 50 cm), the scores were 0.06, 0.11, 0.33, 0.44 and 0.62, respectively. It is evident that a greater depth of polymer mixing in the soil corresponded to a higher score. Moreover, the highest-scoring treatment significantly outperformed the lowest-scoring one, emphasizing the substantial impact of optimizing the mixing depth on overall benefits. Overall, in polymer management, it is crucial to comprehensively consider both the rate and depth of polymer application.

Table 3. Evaluation of polymer comprehensive benefits based on TOPSIS.

Application Rate (%)	Maximum Mixing Depths (cm)	D^+	D^-	Scores	Ranking
0.00	50	0.65	0.67	0.51	3
0.15	50	0.51	0.60	0.54	2
0.30	50	0.42	0.69	0.62	1
0.45	50	0.53	0.54	0.51	4
0.60	50	0.71	0.62	0.47	5
0.30	10	0.96	0.06	0.06	9
0.30	20	0.90	0.11	0.11	8
0.30	30	0.70	0.35	0.33	7
0.30	40	0.58	0.45	0.44	6
0.30	50	0.42	0.69	0.62	1

A binary quadratic equation proved to be more effective in describing the influence of polymer application rate and depth on comprehensive evaluation scores (Figure 10). Considering that the root of most crops rarely extended beyond 50 cm, the maximum mixing depth was set at 50 cm. Utilizing Matlab software for simulation and optimization of the regression model, the highest score was achieved when the polymer was uniformly distributed at a rate of 0.27% in the soil layer of 0–50 cm. In contrast, the lowest score was obtained with a mixing depth of 0–10 cm and an application rate of 0.60%. Therefore, it can be concluded that the optimal polymer management strategy was an application rate of 0.27% with a mixing depth of 0–50 cm.

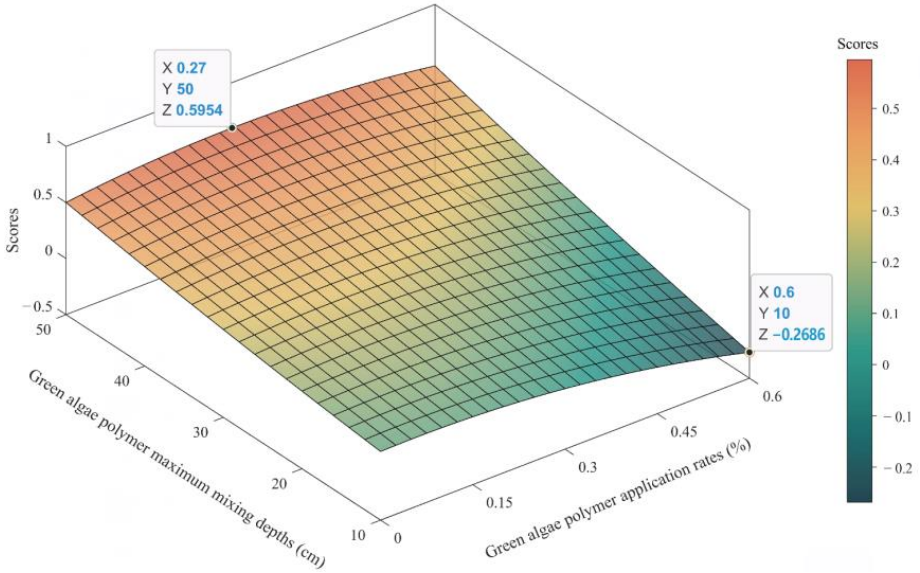

Figure 10. Effect of application rate and maximum mixing depth interaction on comprehensive score of polymer management.

4. Discussion

4.1. Swelling Performance of Polymers Prepared from Green Algae

Eutrophication of water bodies is one of the major significant environmental problems faced globally. One of its main manifestations is green algae bloom, which is generated

in alarming amounts worldwide each year. It has been reported that the annual global production of green algae causes a huge burden on the environment. Currently, the handling of green algae waste poses a considerable challenge and requires significant resources. Therefore, it is imperative to explore and implement sustainable approaches for the management of green algae [43].

Green algae are abundant in cellulose, a natural polymer containing numerous hydrophilic groups. In the presence of an initiator, free radicals are formed in the cellulose macromolecular structure, reacting with monomers to create graft copolymers with exceptional water absorption capabilities [43]. In this study, we successfully synthesized a polymer with remarkable water absorption properties by polymerizing green algae in conjunction with acrylic acid and other substances. Its swelling rate of 143.6 g/g was very close to the previous polymers derived from cellulose [44]. Wang et al. [45] reported that the swelling rate of polymers prepared from corn stover cellulose was in the range of 103.5–297.36 g/g. Evidently, the swelling rate of this particular polymer was indeed lower when compared to conventional polymers, which typically exhibited a range of 400–1000 g/g. This difference might be related to the variation in raw materials [11,46]. In general, depending on the synthetic material used, water retention agents can be classified into: synthetic resin-based polymer, starch-based polymer and cellulose-based polymer [9]. Among these, cellulose-based polymers exhibited a lower swelling rate, primarily due to differences in their molecular and pore structures [47,48]. Resin and starch polymers were usually composed of linear or branched polymer compounds with a more open molecular structure, favoring the formation of a large number of pores and water-absorbing channels, resulting in a high swelling rate [49]. In contrast, the molecular structure of cellulose exhibited a certain degree of crystallinity and was more compact, impeding the penetration and adsorption of water molecules and resulting in a weaker swelling rate [50]. In addition, the small and few pores in the cellulose-based polymer structure restricted the entry and storage of water molecules, further reducing swelling rate. The crystalline and fibrous morphology of cellulose also caused slow diffusion of water molecules through the cellulose structure, resulting in a relatively slow swelling process. In this study, the green algal polymer took 120 min to reach swelling equilibrium (Figure 5). Despite these disadvantages, cellulose polymers had high compressive strength, fewer soluble components, and longer service life compared to starch-based products that suffer from inadequate long-term water retention and susceptibility to microbial decomposition [51]. This study yielded similar findings. While the swelling rate gradually declined with repeated reswelling, it eventually stabilized after the fifth reswelling, demonstrating good repeatability (Figure 5). Additionally, when exposed to high temperatures, the swelling rate decreased but retained its water retention properties to a considerable extent, indicating high-temperature stability (Figure 6). Overall, cellulose-based polymers have slightly lower water absorption, but are stable and biodegradable, thereby possessing significant potential for further development. Consequently, transforming green algae into polymers that can benefit agricultural production emerges as a win–win strategy, converting waste into a valuable resource. This approach not only addresses the challenge of green algae disposal but also provides an efficient water retention solution for arid zone agriculture by significantly increasing crop yields and WUE [1,11,52].

4.2. Effects of Green Algal Polymer on Soil Infiltration and Evaporation

Water-holding agents improve plant growth, yield and WUE, mainly by enhancing soil moisture conditions, especially through the effect on infiltration [53]. In this study, the transport of wetting front gradually slowed with the increasing polymer application rates (Figure 7a). This might be caused by two factors: (i) the addition of polymers increased the saturated soil water content, and (ii) the polymers absorbed water and swelled to block the soil pore space, resulting in a slower wetting front migration [19]. A similar phenomenon was observed at different maximum mixing depths. As the maximum mixing depth increased, the wetting front transport accelerated. This phenomenon could be attributed to

the higher polymer content in the surface layer when the maximum mixing depth was shallow. For instance, at a maximum mixing depth of 10 cm, the polymer content from 0 to 10 cm was 1.5%. Consequently, the saturation of water content and pore plugging significantly increased, hindering the wetting front transport and leading to prolonged infiltration. Moreover, although higher polymer application rates increased cumulative infiltration, the average infiltration rate declined with increasing polymer application rates due to the prolonged infiltration duration (Figure 8). These findings were in line with previous studies [36]. In summary, the polymer reduced the wetting front transport and infiltration rate, but increased the cumulative infiltration, and the wetting front transport process and cumulative infiltration could be simulated by the power function and Horton models.

Reducing water loss through evaporation is a crucial measure to improve crop production and WUE [54]. It is estimated that nearly 83% of rainfall evaporates shortly after precipitation, while the remaining 14% infiltrates into dry soil and is utilized by natural vegetation [15]. Soil evaporation is primarily influenced by atmospheric evapotranspiration forces and soil water transport capacity. When the soil contained water-retaining agents, on the one hand, the higher water content increased the specific heat capacity, hindering the downward transmission of air energy. On the other hand, the soil pores were blocked, resulting in a blockage of the "water channel" for the upward transport of evaporated water. Consequently, as the amount of polymer application rate increased, the evaporation gradually decreased (Figure 8). At a 0.3% application rate, the cumulative evapotranspiration was observed to be 31.7 mm, significantly lower than the CK treatment, which recorded 36.9 mm. However, with a further increase in polymer application rate, cumulative evapotranspiration showed an upward trend, possibly due to the higher soil water content under high polymer. This indicates that the inhibitory effect of polymers on evaporation increased and then decreased with the amount used, which aligned with a previous study by Xiong [35]. Xiong demonstrated that the anti-evaporation effect of hydrogel in soil followed a similar pattern, with the best anti-evaporation effect observed at a hydrogel content of 0.10%. Overall, while polymers increased cumulative soil infiltration, excessive application of polymers to shallow soils resulted in significant evaporation loss. Therefore, it is essential to determine the optimum amount and depth of polymer to minimize evaporation and improve soil moisture conditions.

4.3. Effects of Polymer Management on Overall Benefits

Water-retaining agents have gained widespread use in agricultural systems due to their ability to enhance soil moisture effectiveness, alleviate water scarcity's negative impacts, and increase agronomic traits [55,56]. It is crucial to note that the efficacy of these polymers is contingent on the amount utilized. Jnanesha et al. [57] revealed that increased polymer usage significantly enhanced crop WUE. Liang et al. [58] established a secondary relationship between water-retaining agent application and WUE in cotton fields of southern Xinjian, recommending an optimal 80 kg/ha γ-PGA application rate. In addition, research has shown that combining polymers with deficit irrigation could maximize WUE [10,59]. Variations in research outcomes might be linked to polymers' effects on cumulative infiltration and evaporation. As polymer usage increased, cumulative infiltration also increased, while evaporation initially decreased and then rose. This interplay between high application rates and increased evaporation might influence the overall effectiveness of polymers. In the present study, a comprehensive analysis of infiltration rate, cumulative infiltration, and evaporation characteristics was employed to evaluate the overall benefits of polymers at different application rates and mixing depths using the TOPSIS method. The results favored uniform mixing at a 0.27% application rate in the 0–50 cm soil layer as the optimal management (Figure 10). Furthermore, the study indicated that mixing depth significantly influenced comprehensive benefits compared to application rate. However, it is noteworthy that limited research has been conducted on the optimal maximum mixing depth, calling for further investigation and optimization in subsequent studies.

4.4. Limitations

The swelling rate of the polymer in this study was 143.6 g/g, leaving significant room for improvement. Wang et al. [44] demonstrated that the amount of cross-linking agent significantly affects water absorption. Excessively high levels of cross-linker led to the formation of additional networks and reduced available free volume, thereby decreasing water absorption. Conversely, excessively low levels of cross-linking agent decreased crosslinking density and increased soluble substances, also resulting in decreased water absorption. The initiator has a similar effect [25]. In this study, we did not explore the effect of cross-linking agents as well as other reagents on the swelling properties, which could be further explored in subsequent studies. Additionally, while cellulosic polymers are generally considered biocompatible. The specific degradability and degradation cycle were not examined in this study. Careful substantiation is needed for practical applications. Furthermore, in this study, we established polymer management strategies based on infiltration rate, cumulative infiltration, and evapotranspiration. However, the effects of polymer action on soil type, irrigation, and crop rooting factors are closely related and need specific analysis for particular conditions in subsequent studies [10].

Generally, water retention polymers are more effective and demanded in water-scarce areas [60]. Previous studies in northern China have shown that water retention polymers could significantly improve WUE and yield in maize and wheat [61,62]. For instance, Islam et al. [63] demonstrated that maize yield increased significantly by 22.4% and 27.8% after application of 30 and 40 kg/ha superabsorbent polymer, respectively, in the arid region of northern China. In this study, it was confirmed that the synthesized green algae polymer had good theoretical water retention performance, providing a basis for their practical application in the field. In future studies, it is necessary to continue exploring the water retention performance of the synthesized polymers in field applications, especially in maize and wheat cultivation in the arid and rainless northern China.

5. Conclusions

A polymer with a swelling rate of 143.6 g/g was successfully prepared using waste green algae, exhibiting both reusability and excellent temperature stability. Increasing polymer application rate led to a reduction in wetting front transport, infiltration rate, and an increase in cumulative infiltration. The trend of cumulative evapotranspiration displayed an initial decrease followed by an increase with higher polymer application rates. Additionally, an increase in maximum mixing depth resulted in an acceleration in wetting front transport, infiltration rate, and cumulative infiltration, whereas evaporation decreased. Based on comprehensive consideration of cumulative infiltration, infiltration rate, and evaporation characteristics, an optimized polymer application rate of 0.27% and mixing depth of 0–50 cm are recommended for efficient soil moisture management. Our findings mark a crucial step towards harnessing the potential of green algae as a valuable resource in achieving sustainable and water-saving agricultural practices, which suggests practical methods and implementation strategies for enhancing wheat and maize yields and WUE in arid, low rainfall areas of northern China.

Author Contributions: Z.H. and J.L. conceived and designed the experiments. Z.H. performed the experiments, analyzed and interpreted the data and results, and wrote the original manuscript. C.L. and D.W performed the experiments and analyzed and interpreted the data and results. D.W. and Y.L. provided materials, instrument facilities and monitored the experimental work. J.L., Y.L. and Q.Y. revised the manuscript and gave valuable input. All authors have read and agreed to the published version of the manuscript.

Funding: This study was supported by the Fundamental Research Funds for the Central Universities, CHD (grant 300102292506) and the National Natural Science Foundation of China (grant number: 52209055).

Data Availability Statement: The data presented in this study are available on request from the corresponding author.

Acknowledgments: We appreciate Shuyao Pei and Chen Qi very much for their kind help in conducting the experiment, sampling, and pretreatment of samples.

Conflicts of Interest: The authors declare no conflict of interest.

References

1. Zheng, H.; Mei, P.; Wang, W.; Yin, Y.; Li, H.; Zheng, M.; Ou, X.; Cui, Z. Effects of super absorbent polymer on crop yield, water productivity and soil properties: A global meta-analysis. *Agric. Water Manag.* **2023**, *282*, 108290. [CrossRef]
2. Mazhar, M.W.; Ishtiaq, M.; Maqbool, M.; Akram, R. Seed priming with Calcium oxide nanoparticles improves germination, biomass, antioxidant defence and yield traits of canola plants under drought stress. *S. Afr. J. Bot.* **2022**, *151*, 889–899. [CrossRef]
3. Albalasmeh, A.A.; Mohawesh, O.; Gharaibeh, M.A.; Alghamdi, A.G.; Alajlouni, M.A.; Alqudah, A.M. Effect of hydrogel on corn growth, water use efficiency, and soil properties in a semi-arid region. *J. Saudi Soc. Agric. Sci.* **2022**, *21*, 518–524. [CrossRef]
4. Mi, J.; Gregorich, E.G.; Xu, S.; McLaughlin, N.B.; Ma, B.; Liu, J. Effect of bentonite amendment on soil hydraulic parameters and millet crop performance in a semi-arid region. *Field Crops Res.* **2017**, *212*, 107–114. [CrossRef]
5. Ahmed, E.M. Hydrogel: Preparation, characterization, and applications: A review. *J. Adv. Res.* **2015**, *6*, 105–121. [CrossRef] [PubMed]
6. Al-Jabari, M.; Ghyadah, R.A.; Alokely, R. Recovery of hydrogel from baby diaper wastes and its application for enhancing soil irrigation management. *J. Environ. Manag.* **2019**, *239*, 255–261. [CrossRef]
7. AbdAllah, A.M.; Mashaheet, A.M.; Burkey, K.O. Super absorbent polymers mitigate drought stress in corn (*Zea mays* L.) grown under rainfed conditions. *Agric. Water Manag.* **2021**, *254*, 106946. [CrossRef]
8. Verma, A.K.; Sindhu, S.S.; Singh, A.; Kumar, A.; Singh, A.; Chauhan, V.B.S. Conditioning effects of biodegradable superabsorbent polymer and vermi-products on media properties and growth of gerbera. *Ecol. Eng.* **2019**, *132*, 23–30. [CrossRef]
9. Ai, F.; Yin, X.; Hu, R.; Ma, H.; Liu, W. Research into the super-absorbent polymers on agricultural water. *Agric. Water Manag.* **2021**, *245*, 106513. [CrossRef]
10. Satriani, A.; Catalano, M.; Scalcione, E. The role of superabsorbent hydrogel in bean crop cultivation under deficit irrigation conditions: A case-study in Southern Italy. *Agric. Water Manag.* **2018**, *195*, 114–119. [CrossRef]
11. Chang, L.; Xu, L.; Liu, Y.; Qiu, D. Superabsorbent polymers used for agricultural water retention. *Polym. Test.* **2021**, *94*, 107021. [CrossRef]
12. Xie, X.; Ma, L.; Chen, Y.; Luo, X.; Long, M.; Ji, H.; Chen, J. Bagasse cellulose composite superabsorbent material with double-crosslinking network using chemical modified Nano-$CaCO_3$ reinforcing strategy. *Nanomaterials* **2022**, *12*, 1459. [CrossRef] [PubMed]
13. Chamizo, S.; Cantón, Y.; Rodríguez-Caballero, E.; Domingo, F.; Escudero, A. Runoff at contrasting scales in a semiarid ecosystem: A complex balance between biological soil crust features and rainfall characteristics. *J. Hydrol.* **2012**, *452–453*, 130–138. [CrossRef]
14. Cui, Z.; Huang, Z.; Luo, J.; Qiu, K.; López-Vicente, M.; Wu, G.-L. Litter cover breaks soil water repellency of biocrusts, enhancing initial soil water infiltration and content in a semi-arid sandy land. *Agric. Water Manag.* **2021**, *255*, 107009. [CrossRef]
15. Song, M.; Lin, S.; Takahashi, F. Coal fly ash amendment to mitigate soil water evaporation in arid/semi-arid area: An approach using simple drying focusing on sieve size and temperature. *Resour. Conserv. Recycl.* **2020**, *156*, 104726. [CrossRef]
16. Misiewicz, J.; Datta, S.S.; Lejcuś, K.; Marczak, D. The characteristics of time-dependent changes of coefficient of permeability for superabsorbent polymer-soil mixtures. *Materials* **2022**, *15*, 4465. [CrossRef] [PubMed]
17. Han, Y.G.; Yang, P.L.; Luo, Y.P.; Ren, S.M.; Zhang, L.X.; Xu, L. Porosity change model for watered super absorbent polymer-treated soil. *Environ. Earth Sci.* **2010**, *61*, 1197–1205. [CrossRef]
18. Guo, J.; Shi, W.; Wen, L.; Shi, X.; Li, J. Effects of a super-absorbent polymer derived from poly-γ-glutamic acid on water infiltration, field water capacity, soil evaporation, and soil water-stable aggregates. *Arch. Agron. Soil Sci.* **2020**, *66*, 1627–1638. [CrossRef]
19. Zhao, W.; Hu, J.; Cui, Z.; Dou, P.; Fan, Y. Effects of superabsorbent polymers on the vertical infiltration of soil water with sand mulching. *Environ. Earth Sci.* **2019**, *78*, 648. [CrossRef]
20. Bai, W.; Li, M.; Zhao, H.; Liu, B.; Wu, Y.; Song, J. Effect of super absorbent polymer on the ponding infiltration characteristics of soil water. *Chin. Agric. Sci.* **2010**, *43*, 5055–5062.
21. Zhao, W.; Cao, T.; Dou, P.; Sheng, J.; Luo, M. Effect of various concentrations of superabsorbent polymers on soil particle-size distribution and evaporation with sand mulching. *Sci. Rep.* **2019**, *9*, 3511. [CrossRef] [PubMed]
22. Yu, J.; Shi, J.G.; Ma, X.; Dang, P.F.; Yan, Y.L.; Mamedov, A.I.; Shainberg, I.; Levy, G.J. Superabsorbent polymer properties and concentration effects on water retention under drying conditions. *Soil Sci. Soc. Am. J.* **2017**, *81*, 889–901. [CrossRef]
23. Yang, L.; Han, Y.; Yang, P.; Wang, C.; Yang, S.; Kuang, S.; Yuan, H.; Xiao, C. Effects of superabsorbent polymers on infiltration and evaporation of soil moisture under point source drip irrigation. *Irrig. Drain.* **2015**, *64*, 275–282. [CrossRef]
24. Chen, Y.; Tang , H.; Liu , Y.; Tan, H. Preparation and study on the volume phase transition properties of novel carboxymethyl chitosan grafted polyampholyte superabsorbent polymers. *J. Taiwan Inst. Chem. Eng.* **2016**, *59*, 569–577. [CrossRef]
25. Fang, S.; Wang, G.; Li, P.; Xing, R.; Liu, S.; Qin, Y.; Yu, H.; Chen, X.; Li, K. Synthesis of chitosan derivative graft acrylic acid superabsorbent polymers and its application as water retaining agent. *Int. J. Biol. Macromol.* **2018**, *115*, 754–761. [CrossRef]
26. Zhang, M.; Zhang, S.; Chen, Z.; Wang, M.; Cao, J.; Wang, R. Preparation and characterization of superabsorbent polymers based on sawdust. *Polymers* **2019**, *11*, 1891. [CrossRef]

27. Qin, B.; Li, W.; Zhu, G.; Zhang, Y.; Wu, T.; Gao, G. Cyanobacterial bloom management through integrated monitoring and forecasting in large shallow eutrophic Lake Taihu (China). *J. Hazard. Mater.* **2015**, *287*, 356–363. [CrossRef]
28. Amorim, C.A.; Moura, A.d.N. Ecological impacts of freshwater algal blooms on water quality, plankton biodiversity, structure, and ecosystem functioning. *Sci. Total Environ.* **2021**, *758*, 143605. [CrossRef]
29. Yu, Q.; Chen, Y.; Liu, Z.; De Giesen, N.V.; Zhu, D. The Influence of a Eutrophic Lake to the River Downstream: Spatiotemporal Algal Composition Changes and the Driving Factors. *Water* **2015**, *7*, 2184–2201. [CrossRef]
30. Yang, F.; Li, G.; He, Y.-G.; Ren, F.-X.; Wang, G.-X. Synthesis, characterization, and applied properties of carboxymethyl cellulose and polyacrylamide graft copolymer. *Carbohydr. Polym.* **2009**, *78*, 95–99. [CrossRef]
31. Ashkani, M.; Bouhendi, H.; Kabiri, K.; Rostami, M.R. Synthesis of poly (2-acrylamido-2-methyl propane sulfonic acid) with high water absorbency and absorption under load (AUL) as concrete grade superabsorbent and its performance. *Constr. Build. Mater.* **2019**, *206*, 540–551. [CrossRef]
32. Zhang, C.; García Meza, J.V.; Zhou, K.; Liu, J.; Song, S.; Zhang, M.; Meng, D.; Chen, J.; Xia, L.; Xiheng, H. Superabsorbent polymer used for saline-alkali soil water retention. *J. Taiwan Inst. Chem. Eng.* **2023**, *145*, 104830. [CrossRef]
33. Zhang, J.-P.; Zhang, F.-S. Recycling waste polyethylene film for amphoteric superabsorbent resin synthesis. *Chem. Eng. J.* **2018**, *331*, 169–176. [CrossRef]
34. Cheng, S.; Liu, X.; Zhen, J.; Lei, Z. Preparation of superabsorbent resin with fast water absorption rate based on hydroxymethyl cellulose sodium and its application. *Carbohydr. Polym.* **2019**, *225*, 115214. [CrossRef] [PubMed]
35. Xiong, H.; Peng, H.; Ye, X.e.; Kong, Y.; Wang, N.; Yang, F.; Meni, B.-H.; Lei, Z. High salt tolerance hydrogel prepared of hydroxyethyl starch and its ability to increase soil water holding capacity and decrease water evaporation. *Soil Tillage Res.* **2022**, *222*, 105427. [CrossRef]
36. Zhang, W.; Wang, P.; Deng, Y.; He, X.; Yang, X.; Chen, R.; Lei, Z. Preparation of superabsorbent polymer gel based on PVPP and its application in water-holding in sandy soil. *J. Environ. Chem. Eng.* **2021**, *9*, 106760. [CrossRef]
37. Liu, Z.; Cai, L.; Dong, Q.; Zhao, X.; Han, J. Effects of microplastics on water infiltration in agricultural soil on the Loess Plateau, China. *Agric. Water Manag.* **2022**, *271*, 107818. [CrossRef]
38. Wang, Z.C.; Zhang, B.W.; Ni, J.X.; Yang, W.H.; Li, W.P. Effect of Microplastics on Soil Water Infiltration and Evaporation. *Environ. Sci.* **2022**, *43*, 4394–4401.
39. Wang, Z.; Li, X.; Shi, H.; Zhang, D.; Xu, P. Effects of residual plastic film on infiltration and evaporation for sandy loam and sandy soil. *Trans. Chin. Soc. Agric. Mach.* **2017**, *48*, 198–205.
40. Liu, L.; Fei, L.; Zhu, H.; Hao, K.; Jie, F. Study on the influence of fertilizer solution concentration on soil water and nitrogen transport characteristics under film hole irrigation. *J. Soil Sci. Plant Nutr.* **2021**, *21*, 1653–1665. [CrossRef]
41. Swartzendruber, D. Revised attribution of the power form infiltration equation. *Water Resour. Res.* **1993**, *29*, 2455–2456. [CrossRef]
42. Liu, J.; Xie, M.; Chen, S.; Xu, G.; Wu, T.; Li, W. TS-REPLICA: A novel replica placement algorithm based on the entropy weight TOPSIS method in spark for multimedia data analysis. *Inf. Sci.* **2023**, *626*, 133–148. [CrossRef]
43. Mihranyan, A. Cellulose from cladophorales green algae: From environmental problem to high-tech composite materials. *J. Appl. Polym. Sci.* **2011**, *119*, 2449–2460. [CrossRef]
44. Wang, W.; Yang, Z.; Zhang, A.; Yang, S. Water retention and fertilizer slow release integrated superabsorbent synthesized from millet straw and applied in agriculture. *Ind. Crops Prod.* **2021**, *160*, 113126. [CrossRef]
45. Wang, Y.; Wang, Y.; Wang, P. Synthesis and characterization of corn straw residue water retention agent. *Trans. Chin. Soc. Agric. Mach.* **2016**, *47*, 199–206.
46. Zhang, W.; Wang, P.; Liu, S.; Chen, J.; Chen, R.; He, X.; Ma, G.; Lei, Z. Factors affecting the properties of superabsorbent polymer hydrogels and methods to improve their performance: A review. *J. Mater. Sci.* **2021**, *56*, 16223–16242. [CrossRef]
47. Zhao, C.; Zhang, M.; Liu, Z.; Guo, Y.; Zhang, Q. Salt-tolerant superabsorbent polymer with high capacity of water-nutrient retention derived from sulfamic acid-modified starch. *ACS Omega* **2019**, *4*, 5923–5930. [CrossRef]
48. Haraguchi, K.; Li, H.-J.; Matsuda, K.; Takehisa, T.; Elliott, E. Mechanism of forming organic/inorganic network structures during in-situ free-radical Polymerization in PNIPA—Clay nanocomposite hydrogels. *Macromolecules* **2005**, *38*, 3482–3490. [CrossRef]
49. Zou, W.; Yu, L.; Liu, X.; Chen, L.; Zhang, X.; Qiao, D.; Zhang, R. Effects of amylose/amylopectin ratio on starch-based superabsorbent polymers. *Carbohydr. Polym.* **2012**, *87*, 1583–1588. [CrossRef]
50. Song, J.; Zhao, H.; Zhao, G.; Xiang, Y.; Liu, Y. Novel Semi-IPN Nanocomposites with Functions of both Nutrient Slow-Release and Water Retention. 1. Microscopic Structure, Water Absorbency, and Degradation Performance. *J. Agric. Food Chem.* **2019**, *67*, 7587–7597. [CrossRef]
51. Li, X.; Li, Q.; Su, Y.; Yue, Q.; Gao, B.; Su, Y. A novel wheat straw cellulose-based semi-IPNs superabsorbent with integration of water-retaining and controlled-release fertilizers. *J. Taiwan Inst. Chem. Eng.* **2015**, *55*, 170–179. [CrossRef]
52. Zhao, C.; Zhang, L.; Zhang, Q.; Wang, J.; Wang, S.; Zhang, M.; Liu, Z. The effects of bio-based superabsorbent polymers on the water/nutrient retention characteristics and agricultural productivity of a saline soil from the Yellow River Basin, China. *Agric. Water Manag.* **2022**, *261*, 107388.
53. Xiao, B.; Sun, F.; Hu, K.; Kidron, G.J. Biocrusts reduce surface soil infiltrability and impede soil water infiltration under tension and ponding conditions in dryland ecosystem. *J. Hydrol.* **2019**, *568*, 792–802. [CrossRef]

54. Wang, F.; Zhang, X.; Neal, A.L.; Crawford, J.W.; Mooney, S.J.; Bacq-Labreuil, A. Evolution of the transport properties of soil aggregates and their relationship with soil organic carbon following land use changes. *Soil Tillage Res.* **2022**, *215*, 105226. [CrossRef]
55. Zhu, J.; Suhaimi, F.; Lim, J.Y.; Gao, Z.; Swarup, S.; Loh, C.S.; Li, J.; Ong, C.N.; Tan, W.K. A field study on using soybean waste-derived superabsorbent hydrogel to enhance growth of vegetables. *Sci. Total Environ.* **2022**, *851*, 158141. [CrossRef]
56. Bana, R.S.; Grover, M.; Singh, D.; Bamboriya, S.D.; Godara, S.; Kumar, M.; Kumar, A.; Sharma, S.; Shekhawat, P.S.; Lomte, D.; et al. Enhanced pearl millet yield stability, water use efficiency and soil microbial activity using superabsorbent polymers and crop residue recycling across diverse ecologies. *Eur. J. Agron.* **2023**, *148*, 126876. [CrossRef]
57. Jnanesha, A.C.; Kumar, A.; Lal, R.K. Hydrogel application improved growth and yield in Senna (*Cassia angustifolia* Vahl. *). Ind. Crops Prod.* **2021**, *174*, 114175. [CrossRef]
58. Liang, J.; Shi, W.; He, Z.; Pang, L.; Zhang, Y. Effects of poly-γ-glutamic acid on water use efficiency, cotton yield, and fiber quality in the sandy soil of southern Xinjiang, China. *Agric. Water Manag.* **2019**, *218*, 48–59. [CrossRef]
59. Zinivand, N.; Khodadadi-Dehkordi, D.; Kashkuli, H.A.; Asareh, A.; Egdernezhad, A. Assessment of superabsorbent polymer effect on water use efficiency of plant under water deficit conditions. *Tecnol. Cienc. Agua.* **2020**, *11*, 315–341.
60. Jahan, M.; Nassiri Mahallati, M. Can Superabsorbent Polymers Improve Plants Production in Arid Regions? *Adv. Polym. Technol.* **2020**, *2020*, 7124394. [CrossRef]
61. Yang, W.; Guo, S.W.; Li, P.F.; Song, R.Q.; Yu, J. Foliar antitranspirant and soil superabsorbent hydrogel affect photosynthetic gas exchange and water use efficiency of maize grown under low rainfall conditions. *J. Sci. Food Agric.* **2019**, *99*, 350–359. [CrossRef] [PubMed]
62. Bo, Z.; Renkuan, L.; Yunkai, L.; Tao, G.; Peiling, Y.; Ji, F.; Weimin, X.; Zhichao, Z. Water-absorption characteristics of organic–inorganic composite superabsorbent polymers and its effect on summer maize root growth. *J. Appl. Polym. Sci.* **2012**, *126*, 423–435. [CrossRef]
63. Islam, M.R.; Zeng, Z.; Mao, J.; Eneji, A.E.; Xue, X.; Hu, Y. Feasibility of summer corn (*Zea mays* L.) production in drought affected areas of northern China using water-saving superabsorbent polymer. *Plant Soil Environ.* **2011**, *57*, 279–285. [CrossRef]

Disclaimer/Publisher's Note: The statements, opinions and data contained in all publications are solely those of the individual author(s) and contributor(s) and not of MDPI and/or the editor(s). MDPI and/or the editor(s) disclaim responsibility for any injury to people or property resulting from any ideas, methods, instructions or products referred to in the content.